Numerical Simulation of Light Propagation in Plastic Optical Fibres of Arbitrary 3D Geometry

F. JIMÉNEZ [1], J. ARRUE [2], G. ALDABALDETREKU [2], J. ZUBIA [2]
Departments of [(1)]Applied Mathematics and of [(2)]Electronics and Telecommunications
University of the Basque Country UPV/EHU
Escuela Técnica Superior de Ingeniería, Alda. Urquijo s/n, 48013 Bilbao
SPAIN

Abstract: - This paper describes an efficient implementation of numerical algorithms that allows the ray-tracing method to simulate light propagation in step-index plastic optical fibres (POFs) of arbitrary three-dimensional fibre-axis and cross-section geometries. The flexibility provided by this new technique can be very useful for calculating the transmission properties of bent POFs in many complex configurations common in the automotive industry, LANs, sensors, etc. Implementation details of the algorithms are given, followed by a few results to show the agreement with experimental measurements.

Key-Words: - Numerical Methods, Computational Simulation, Geometric Algorithms, Ray-Tracing Method, Plastic Optical Fibres, POF.

1 Introduction

Plastic optical fibres (POFs) present multiple advantages over their glass counterparts: they are more flexible, easier to handle and splice, and cheaper to manufacture. Thanks to the successive improvements in their transparency and bandwidth, industry and researchers have been increasingly interested in them. Many of the research efforts are related with the computational simulation of their performance under different configurations, in order to best exploit their remarkable characteristics. However, some geometric set-ups of practical interest have not been sufficiently studied yet. This paper shows how to apply the ray-tracing technique, which is based on geometric optics [1], to simulate .

At present, POFs serve as a complement for glass fibres in many short-haul communications links, often constituting the solution of choice when there are large numbers of splices to interconnect multiple nearby devices, like in buildings, robots or vehicles [2]. In such applications, an important amount of power loss can arise from bending losses. Most of the times these losses are undesirable, but there are also cases in which they are very useful to design optical devices like sensors based on light power modulation by an external agent [3]. Desirable or not, it is important to be able to compute power losses at the design stage of many devices and layouts, as well as other parameters like light angular distribution, delay times (which affect bandwidth), etc., since such parameters can be greatly affected by the shape of bends and the relative position of each bend with respect to the others in the optical link [4].

According to the refractive index profile inside POFs, these can be divided into step-index (SI), graded index (GI) and multi-step-index (MSI) POFs [5]. SI POFs are the most widely used type of POF nowadays. In them, the refractive index is uniform inside the core, which is surrounded by a cladding of lower refractive index, so rays propagate along the fibre undergoing successive reflections at the core-cladding interface [1]. We can reasonably assume that the cladding extends to infinity.

1.1 The Ray-Tracing Method

In an SI POF the light power flow along the core is modelled as rays of infinitesimal cross-section, which can radiate power towards the cladding at their reflection points. For the analysis to be accurate, a sufficiently high number of rays entering the fibre should be considered, typically several tens of thousands [4]. Each ray is initially associated with a small fraction of the total light input power, depending on its direction and point of entrance, in agreement with the angular and radial power distributions of the light source.

Each time a ray reaches the core-cladding interface, a generalized Fresnel transmission coefficient for curved interfaces can be employed to calculate the fraction of power radiated by the ray into the cladding. The remarkable feature of the power transmission coefficient is that it depends only

on the radius of curvature in the plane of incidence and the inclination with respect to the fibre surface [6]. In addition, the length of the ray path should also be recorded in order to apply the fibre attenuation coefficient due to material absorption [1]. The powers of all the rays reaching the end of the fibre are added to obtain the total output power.

2 The fibre geometry module

2.1 Modelling three-dimensionally bent POFs with variable cross-section

Plastic optical fibres can be bent until bend radii start to be comparable with the core diameter, when radiation losses become very significant. For example, with a typical core diameter of about 1mm, bend radii of about 10mm already yield very important power losses (up to 40% of the total input power, depending on the set-up).

Quite precise computational simulations of light propagation in straight and circular POF sections have already been carried out [7]. However, planar bends often have a variable curvature (i.e. they are not circle arcs), and many bends are not even planar, i.e., their fibre symmetry axes have a torsion. This tends to add some difficulty to the problem, for which no computational simulation tool developed until now is flexible enough. Such a simulation software could also be used for optimization purposes.

Another important enhancement over existing POF simulation software is the possibility to model core cross-sections that deviate from circularity and are allowed to change along the fibre axis. This can model fibre imperfections, as well as connecting devices like fibre tapers, etc. Variable cross-sections of homogeneous equation $(x/a)^m + (y/b)^m = 1$, proposed for GI POFs [8], are general enough for many practical uses.

We will now describe a modular software architecture, including implementation details of the corresponding numerical algorithms, to apply the ray-tracing method to the simulation of light propagation in SI POFs of very flexible geometry –namely, of fibre axes following practically any 3D trajectory and of cross-sections whose size, shape and orientation are also allowed to vary in a very general way.

2.2 Implementation

For the sake of flexibility, it is very convenient to define the fibre geometry as a separate software module (typically a "function" written in a programming language). The propagation of light rays will be calculated in an independent function.

To start with, the shape of the fibre symmetry axis must be defined. Calling **c** a point on it, its 3D Cartesian coordinates will be given as a sufficiently smooth vector function $\mathbf{c}(p)$ of a parameter p which, for programming simplicity, does not need to be a natural parameter (length of fibre axis from a given point on it). A single or piecewise analytical expression of $\mathbf{c}(p)$ is not needed either.

The fibre core could now be defined as the locus of all points in space whose distance to the fibre axis is not greater than the core radius r. This is equivalent to defining the core as the envelope of a sphere of radius r whose centre moves along the fibre axis. Another possible approach is to define the fibre core as the sweep of its cross-section, whose centre follows the fibre axis. When the cross-section is a moving circle, one obtains the so-called pipe surfaces [9,10]. In our case, it is practical to model the fibre volume as the sweep of its normal cross-section, especially when the cross-section deviates from perfect circularity.

The unit tangent vector **t** to the fibre axis at **c** is also given as a function $\mathbf{t}(p)$ –which can be approximated numerically if needed–, as well as two unit vectors $\mathbf{x}(p)$ and $\mathbf{y}(p)$, normal to **t** and to each other, providing the directions of the principal axes of the fibre cross-section and the local coordinate system for its equation, namely

$$\left(\frac{x}{a}\right)^m + \left(\frac{y}{b}\right)^m = 1 \qquad (1)$$

The cross-section half axes a and b, as well as the degree of homogeneity m, are also returned by the geometry module as sufficiently smooth functions of p, as illustrated in Fig.1.

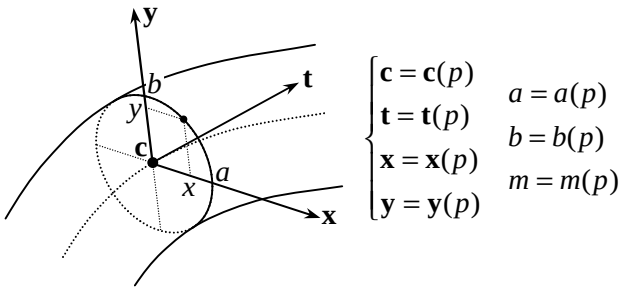

Fig.1: Geometry function returning: centre **c** and tangent **t** of fibre symmetry axis, cross-section main axes $(\mathbf{x}, \mathbf{y})$, half-axes (a, b), degree of homogeneity m.

If $m = 2$, the cross-section is an ellipse; if, additionally, $a = b$, it is a circle. Cross-sections with different equations than (1) are almost as easy to implement, but we will use this for the explanations.

3 The Ray-Tracing module

3.1 Calculation of the reflection points

A ray *r*, defined by any one of its points **r** and its direction **d**, is introduced in the fibre core, and its intersection points with successive fibre cross-sections are calculated to obtain the next reflection point.

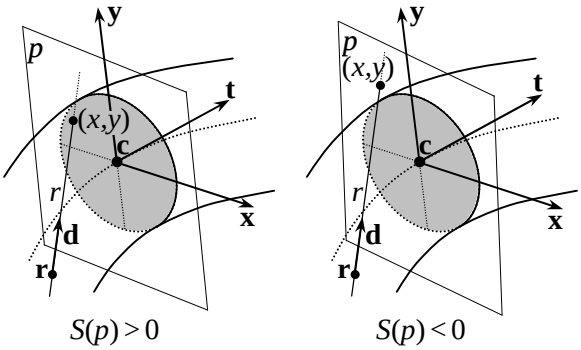

Fig.2: Reflection points obtained by intersecting a ray with successive fibre cross-sections.

For each value of the parameter *p* considered, it is immediate to find out the plane $\pi(p)$ containing the corresponding fibre cross-section, since we know its point **c**(*p*) and its director **t**(*p*). Then, the intersection point between *r* and π is calculated (Fig.2), and its corresponding coordinates in the local coordinate system (*x*,*y*) are obtained. Therefore, for any value of *p*, the following *slack function* –or residue associated with (1)– can be defined and calculated in a straightforward manner:

$$S(p) = 1 - \left(\frac{x(p)}{a(p)}\right)^{m(p)} - \left(\frac{y(p)}{b(p)}\right)^{m(p)}$$

The slack *S*(*p*) provides a certain measurement of the distance of a point on the ray to the fibre core surface. Its value is positive for points inside the fibre core, and negative for points outside it. The objective is therefore to find the first root of *S*(*p*), from which the calculation of the corresponding point $\mathbf{s} = \mathbf{c} + x\,\mathbf{x} + y\,\mathbf{y}$ on the core surface is straightforward.

Since a typical simulation may involve the calculation of 100 million reflection points or more, it is critical to choose an efficient algorithm for numerically solving $S(p) = 0$ with good precision. The method of choice for general one-dimensional root-finding without available derivatives is still widely accepted to be the Van Wijngaarden-Dekker-Brent Method (or simply Brent's method) [11]. It combines sureness of convergence (once the root of the continuous function has been bracketed) with superlinear convergence and careful handling of round-off error propagation.

It is easy to provide Brent's method with two values of *p* where *S*(*p*) has opposite signs. A sufficiently small increase of *p* above its value at any reflection point always produces $S(p) > 0$, while a sufficiently large one produces either $S(p) < 0$ or reaching the fibre end. The difficulty arises when trying to make sure that the roots found are consecutive.

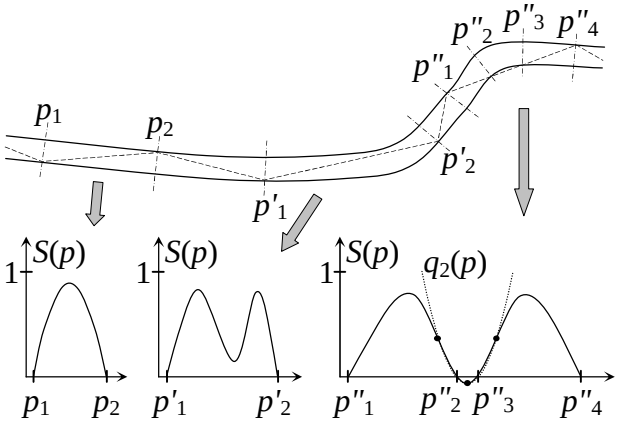

Fig.3: Slack function *S*(*p*) between successive reflection points. Care must be taken not to miss the first root p''_2 after p''_1 and find p''_3 or p''_4 instead.

The evolution of *S*(*p*) between two successive reflection points is schematically shown in Fig.3 for three different typical cases. A two-dimensional representation is enough to illustrate the main issues involved. Most of the times *S*'(*p*) decreases monotonously between two successive reflection points (Fig.3, left), but it is not uncommon for a local minimum of *S*(*p*) to be found inside the interval (Fig.3, centre and right). This happens near fibre bends. In these cases, it is possible to fail to detect the first root in the interval, which would be p''_2, and arrive at p''_3 or p''_4 instead, as can be seen on Fig.3, right.

Careful implementation of algorithms is therefore needed. In the first place, *p* should not be increased too far to provide Brent's method with the second bracketing value. Besides, it is a good idea to monitor the sign of *S*(*p*) at every point in which Brent's method evaluates it.

In the second place, it should be checked that $S'(p) < 0$ at every root returned by Brent's method, to discard points of re-entrance of the ray in the fibre such as p''_3 in Fig.3. This can be done either by means of a finite difference, or by calculating the scalar product of the ray director **d** with the outer normal to the fibre surface **n** and checking that it is positive. The latter method is preferable because it is computationally cheaper (since **n** must be calculated anyway) and probably more precise too.

Finally, since a wrong value such as p''_4 in Fig.3 is not so easy to discard as a point of re-entrance such as p''_3, concavity tests should be carried out inside every interval in order to detect a possible local minimum of $S(p)$ and its sign. A simple technique to do so is to perform an inverse parabolic interpolation by choosing three interior nodes on the curve $S(p)$ and obtaining the value p^* where their interpolating quadratic parabola $q_2(p)$ reaches its minimum. Practice shows that this parabolic fit is good enough in almost all cases. A simple search criterion could then be to obtain the absolute difference between $q_2(p^*)$ and $S(p^*)$ and to subtract it from the minimum of the two. If this quantity is negative, a finer search should be performed.

3.2 Normal to the fibre core surface

An important step in the ray-tracing method involves the precise calculation of the normal **n** to the fibre core surface at reflection points. With it, both the reflected ray and the Fresnel power transmission coefficient can be obtained, although the latter requires some extra calculations to determine the local radius of curvature in the plane of incidence.

In our case, the fibre symmetry-axis can follow a three-dimensional curve with or without analytical expression; in contrast, its cross-section is defined by the precise analytical equation (1). Therefore, the best way to obtain **n** is by means of a combination of numerical and analytical techniques.

As is well known from elementary Differential Geometry, a normal **n** to the surface can be obtained as the cross-product of any two tangents $\mathbf{t_1}$ and $\mathbf{t_2}$ to the core surface at the reflection point **s**, i.e., tangents to any two sufficiently smooth curves on the fibre surface intersecting at the reflection point. It is not necessary that $\mathbf{t_1}$ and $\mathbf{t_2}$ are perpendicular to each other, but near-perpendicularity greatly reduces round-off errors. Fig.4 illustrates this idea.

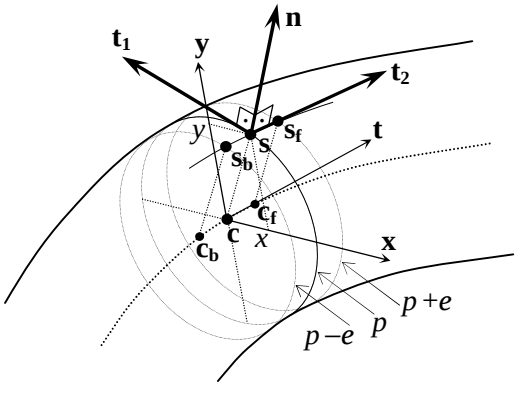

Fig.4: Normal **n** to the fibre surface obtained as the cross-product of any two of its tangents $\mathbf{t_1}$ and $\mathbf{t_2}$.

The first tangent, i.e. tangent $\mathbf{t_1}$ to the cross-section boundary, is obtained analytically in 3D Cartesian coordinates by differentiating (1) implicitly, which yields (in the first quadrant):

$$\frac{dy}{dx} = \frac{-x^{m-1}b^m}{y^{m-1}a^m} \quad \Rightarrow \quad \mathbf{t_1} = k\left(y^{m-1}a^m\,\mathbf{x} - x^{m-1}b^m\,\mathbf{y}\right),$$

and similarly in the other quadrants. This tangent belongs to the plane of the cross-section. It is convenient to choose a consistent sense for $\mathbf{t_1}$ along all the cross-section boundary (e.g. counter-clockwise as in Fig.4) to ensure that the cross-product $\mathbf{n} = \mathbf{t_2}\times\mathbf{t_1}$ always has the same sense (e.g. outward).

The second tangent $\mathbf{t_2}$ is more conveniently obtained numerically. First, the Cartesian coordinates of a reflection point **s** are obtained as $\mathbf{s} = \mathbf{c} + x\,\mathbf{x} + y\,\mathbf{y}$. A small forward increment e of p can yield a similar point $\mathbf{s_f} = \mathbf{c_f} + x_f\,\mathbf{x_f} + y_f\,\mathbf{y_f}$. It is convenient to make $y_f/x_f = y/x$ (with equal signs) so that $\mathbf{t_2}$ is nearly normal to $\mathbf{t_1}$. Then, $\mathbf{t_2}$ can be approximated by the forward finite difference $\mathbf{s_f} - \mathbf{s}$, of first order of precision. Similarly, a backward finite difference $\mathbf{s} - \mathbf{s_b}$ can be used, or the centred finite difference $\mathbf{t_2} = \mathbf{s_f} - \mathbf{s_b}$, which is more precise (second order of precision). Another possibility is to calculate the 3D circle passing through $\mathbf{s_b}$, **s** and $\mathbf{s_f}$, and to approximate $\mathbf{t_2}$ as its tangent at **s**. Care must be taken with round-off errors in all cases.

Finally, **n** is obtained as the cross product $\mathbf{t_2}\times\mathbf{t_1}$, followed by normalization for convenience in later calculations.

3.3 Reflected ray and local radius of curvature in the plane of incidence

The plane of incidence p_i is the one containing the reflection point **s**, the normal to the surface **n** and the ray given by its director **d**, as shown in Fig.5 (left).

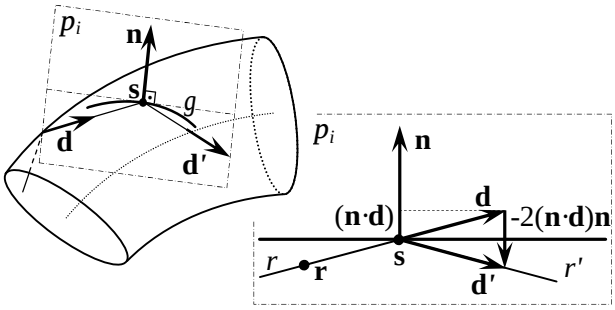

Fig.5: Plane of incidence p_i and ray reflection.

According to Snell's law, if the ray r is reflected (totally or partially) at point **s**, the direction $\mathbf{d}'$ of the reflected ray is calculated as:

$$\mathbf{d}' = \mathbf{d} - 2\,(\mathbf{n}\cdot\mathbf{d})\,\mathbf{n}$$

where all vectors are normalized and **n**·**d** represents the usual scalar product (see Fig.5 right).

The intersection of the plane of incidence p_i with the fibre surface is a curve g whose radius of curvature at **s** is called the local radius of curvature. This radius must be calculated in order to obtain the transmission coefficient, i.e. the fraction of power radiated by the ray into the cladding [6].

One possible way to do so numerically is to obtain the reflection points of two rays in p_i parallel and very close to r (r_1 and r_2 in Fig.6), and then the radius of the circle passing through them and **s**. However, a better way to obtain the local radius of curvature is described next.

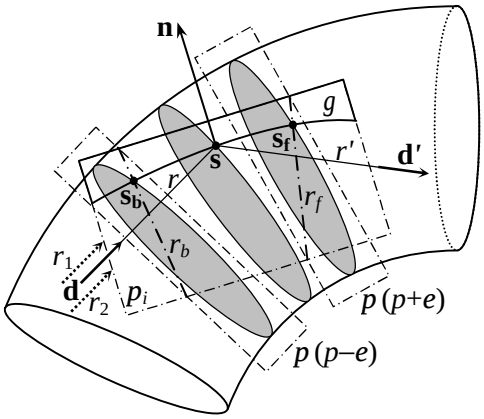

Fig.6: Calculation of the local radius of curvature at the plane of incidence.

Let p be the parameter value at known reflection point $\mathbf{s} = \mathbf{c} + x\,\mathbf{x} + y\,\mathbf{y}$. A small forward increment e is added to p, and the plane $p\,(p+e)$ containing the corresponding cross-section is readily obtained from the geometry module. Its intersection with the plane of incidence p_i, also known, is the straight line r_f (Fig.6). Then, the intersection $\mathbf{s_f}$ of r_f with the fibre cross-section boundary is calculated by writing the equation of r_f in local coordinates as:

$$c_1 x + c_2 y + c_3 = 0 \qquad (2)$$

and solving, together with (1), to yield x_f, y_f, and hence $\mathbf{s_f} = \mathbf{c_f} + x_f\,\mathbf{x_f} + y_f\,\mathbf{y_f}$. An analogous backward increment of p yields $\mathbf{s_b}$. The local radius of curvature sought is then approximated by the radius of the circle passing through $\mathbf{s_b}$, **s** and $\mathbf{s_f}$.

The first advantage of this method over the first one suggested (using rays r_1 and r_2) is that, being r_f and r_b almost perpendicular to the section boundaries at $\mathbf{s_f}$ and $\mathbf{s_b}$ respectively, round-off errors are smaller. The second, more important advantage, is that when the degree of homogeneity in (1) is $m = 2$ (which accounts for circular and elliptical cross-sections, i.e., the majority of cases of practical interest), the system (1)-(2) yields a quadratic equation that can be solved without iterations (which consume most computing time).

4 Some results

The aforementioned algorithms have been implemented in the C programming language, with very good computational times and agreement with experimental results. For example, it only takes about 10 minutes for a 1.3GHz PC to simulate the propagation of 100,000 rays in a 0.49mm POF wrapped two full turns around a 10mm cylinder. We have checked the reliability of the code by comparing its results with those from laboratory measurements. Fig.7 shows that for a cylinder of radius R = 10mm, computational and experimental results nearly coincide, the small difference being due to the difficulty in knowing the exact power distribution of the light source employed (an LED). The agreement is also good for R = 6mm, especially when the number of turns is large, which minimizes the effects of the differences between the modelled and the real light sources. Moreover, to illustrate the three-dimensional capabilities of the program, we have compared the power loss when bending the fibre circularly around a 10mm cylinder with the result obtained when the fibre follows a helix around a 6mm-radius cylinder with the necessary helix-step for the local radius of curvature R to be 10mm as well, maintaining the number of turns. The two results are not equal, as could be expected, because the fibre length is slightly different in both cases and also because the torsion of the helix has a small influence on bending losses.

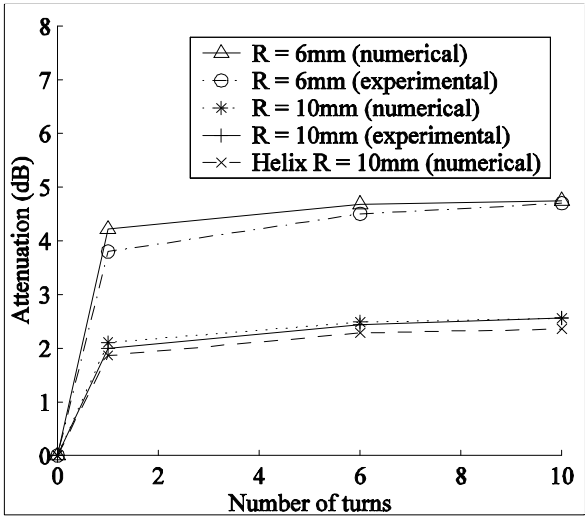

Fig.7: Attenuation induced by fibre bending for different numbers of turns around a cylindrical rod. Computational against experimental results confirm the correct implementation of the algorithms.

5 Further work

Apart from step-index (SI) POFs, graded-index (GI) POFs are also available in the market. In them, the core refractive index decreases smoothly towards the cladding, so a ray propagating inside it does not reflect, but continually refracts following a curved trajectory [8]. Mixed cases also exist, such as the multi-step-index (MSI) POFs, with a core consisting of several concentric layers, each one of constant refractive index [5].

The first natural step to generalize the work described above is to simulate light propagation in MSI POFs. The intersection of a ray with each layer interface can be carried out in the same way as described above. A new difficulty arises because the so-called tunnelling rays [1] that appear in some layers of MSI POFs increase the number of guided rays that must be traced [5].

A second natural line of further work is to simulate light propagation in GI POFs. The numerical techniques to trace the trajectory of a ray will now involve methods to solve systems of ordinary differential equations with initial conditions, like high order Runge-Kutta, predictor-corrector or Bulirsch-Stoer methods with step control [12,13].

A conceptually easier but potentially very useful further work could be a software module that produces the geometry function of a fibre passing through a set of given points. 3D splines could be used to generate $\mathbf{c}(p)$, $\mathbf{t}(p)$, etc. This would be very useful at the design stage of fixed-geometry communications links.

It is also easy to simulate fibres whose cross-section is not described by a homogeneous equation (1). For example, pressing a fibre against a hard surface deforms its cross sections into shapes not considered until now, which can be useful to design pressure sensors by measuring the power attenuation induced. If the cross-section equation is piecewise, it would probably be more convenient to include the computation of the normal $\mathbf{n}(\mathbf{s})$ in the geometry module, rather than in the ray-tracing one.

Finally, the implementation of the ray-tracing method could be made even more efficient by using parallel computing, since the problem structure naturally adapts to it.

6 Conclusions

An efficient implementation of numerical algorithms to simulate light propagation in step-index plastic optical fibres of arbitrary 3D geometry has been described in detail. Its usefulness in practical situations for research and industry has been argued. The quality of its results has been demonstrated by comparison with laboratory measurements. Finally, feasible and useful further work has been proposed.

References:

[1] A. W. Snyder and J. Love, *Optical Waveguide Theory*, Chapman & Hall, 1983.

[2] J. R. Cirillo, K. L. Jennings, M. A. Lynn, D. A. Messuri and R. E. Steele, Local Area Network Applications of Plastic Optical Fiber, *SPIE*, Vol.1592, 1991, pp.42-52.

[3] J. Zubia and J. Arrue, Plastic Optical Fibers: An Introduction to their Technological Processes and Applications, *Optical Fiber Technology*, Vol.7, 2001, pp.101-140.

[4] J. Arrue, J. Zubia, G. Fuster and D. Kalymnios, Light power behaviour when bending plastic optical fibres, *IEE Proc.-Optoelectron.*, Vol.145, No.6, 1998, pp.313-318.

[5] J. Zubia, G. Aldabaldetreku, G. Durana, J. Arrue, H. Poisel and C. A. Bunge, Geometric optics analysis of multi-step index optical fibers, *Fiber and Integrated Optics*, Vol.23, 2004, pp.121-156.

[6] A. W. Snyder and J. D. Love, Reflection at a curved dielectric interface – Electromagnetic Tunneling, *IEEE Trans. Microwave Theory Tech.*, Vol.MTT-23, No.1, 1980, pp.134-141.

[7] J. Marcou and K. Michelet, A new method to evaluate the bends in polymer optical fibers, *Proc. Fifth International Conference on Plastic Optical Fibers and Applications POF'96*, 1996, pp.205-212.

[8] K. F. Barrell and C. Pask, Geometric optics analysis of non-circular, graded-index fibres, *Optical and Quantum Electronics*, Vol.11, 1979, pp.237-251.

[9] T. Maekawa, N. M. Patrikalakis, T. Sakkalis and G. Yu, Analysis and applications of pipe surfaces, *Computer Aided Geometric Design*, Vol.15, No.5, 1998, pp.437-58.

[10] B. Jüttler and M. G. Wagner, Rational motion-based surface generation, *Computer-Aided Design*, Vol.31, 1999, pp.203-213.

[11] R. P. Brent, *Algorithms for Minimization without Derivatives*, Prentice-Hall, 1973.

[12] C. W. Gear, *Numerical Initial Value Problems in Ordinary Differential Equations*, Prentice-Hall, 1971.

[13] J. Stoer and R. Bulirsch, *Introduction to Numerical Analysis*, Springer-Verlag, 1980.